Volume 15, Issue 1, 152509 (1-11)

Iranian Journal of Catalysis (IJC)

https://doi.org/10.57647/j.ijc.2025.1501.09

Synthesis and characterization of CdS and Ni-CdS thin films: An overview of photocatalytic degradation of methylene blue dye

Rajeshvarsing S. Padavi[1,2], Subhash D. Khairnar[1,3], Vinod S. Shrivastava[1]*

[1]*Nano-Chemistry Research Laboratory, G. T. Patil, Arts, Commerce and Science College, Maharashtra, India.*
[2]*RFNS, Senior Science College, Sorapada, Maharashtra, India.*
[3]*SSPM's Vasantrao Naik Arts Science and Commerce College, Nandurbar, Maharashtra, India.*

*__Corresponding author:__ drvinodshrivastava1962@gmail.com

Original Research

Received:
13 October 2024
Revised:
2 December 2024
Accepted:
19 December 2024
Published online:
13 January 2025

Abstract:

CdS and Ni-CdS thin films were synthesized using the chemical bath deposition technique. The samples were characterized by X-ray diffraction (XRD), scanning electron microscopy (SEM), UV-visible diffuse reflectance spectroscopy (UV-DRS), and energy-dispersive X-ray spectroscopy (EDS). The average crystallite size of both thin films ranged between 1.5 to 4.26 nm, analyzed by the XRD as well as the Williamson-Hall method. The SEM results reveal the nanoflakes-like morphology uniformly distributed over the surface of thin films. The optical band gap was decreased from 2.29 to 2.03 eV when Ni^{2+} was incorporated into the CdS crystal lattice. The potential valence and conduction band position of CdS and Ni-CdS thin films was found to be 9.5, 7.7 eV, and 7.2, 5.6 eV, respectively. The synthesized films were used to degrade methylene blue (MB) dye under 160 W mercury vapor lamp irradiation. The degradation rate of MB dye was found to be significantly enhanced when Ni-CdS was used instead of pure CdS in visible light photocatalysis experiments. Degradation efficiency for the CdS thin films was 64% after 120 minutes, while for the Ni-CdS films, it was an impressive 84% after the same amount of time. Incorporating nickel ions into the CdS matrix improved the photocatalytic efficacy by increasing light absorption and decreasing electron-hole recombination. Films doped with Ni showed better photocatalytic activity, as the rate constant (k) for MB degradation rose from 0.028 min^{-1} (CdS) to 0.038 min^{-1} (Ni-CdS).

Keywords: Methylene blue; Thin film; Photocatalysis; Rate constant

1. Introduction

Environmental pollution has become a pressing issue worldwide, growing more severe alongside the swift expansion of industries and the increase in population. The ongoing growth of industries to satisfy the needs of a growing population has resulted in considerable harm to the environment. Urbanization reflects the development of society and has put noteworthiness pressure on our natural resources, which leads to environmental imbalance, i.e., air, soil, and water pollution. Water pollution is a serious issue that affects us all, especially with untreated industrial waste being discharged into our natural water bodies [1–6]. Industries such as textiles, printing, pulp, paper, pharmaceutical, and sugar distillation contribute significantly to the environmental degradation caused by industrial and urban expansion due to their high water demand and harmful waste [7, 8]. The discharge of such industries includes heavy metals, toxic organic and inorganic compounds, and pharmaceutical ingredients, which show adverse effects on both aquatic as well as terrestrial ecosystems [3, 4, 7, 8]. One of the critical aspects of water pollution is the discharge of synthetic dyes from industries, such as dyeing cotton clothing using cationic dyes, which is a major contributor to industrialization-related environmental deterioration, especially in developing nations. Industrial dyes are very stable when exposed to light, heat, and microbiological hazards. These properties make them helpful in manufacturing but

may harm the environment. These dyes color water and deflect sunlight, disrupting aquatic plant photosynthetic processes. Moreover, numerous dyes and their breakdown products pose risks, being toxic, carcinogenic, or mutagenic, which can endanger the health of both aquatic life and humans. Prolonged exposure to water contaminated with dye can cause serious health issues, such as skin irritation, breathing difficulties, and potentially harm to organs [9–11]. However, among the different types of dyes, Methylene blue (MB) is renowned. MB, which is often used in textile and medicinal industries, persists in the environment and accumulates in living organisms. Methemoglobinemia, gastrointestinal problems, and eye burns are some of the potential adverse effects of the widely used dye methylene blue (MB). This situation has led to an environmental crisis that demands immediate focus and sustainable solutions [12–16].

Therefore, wastewater treatment technologies that are effective in removing MB from textile effluent are essential. The traditional biological treatment methods are inadequate for dealing with dye removal and organic pollutant degradation. Semiconductor photocatalysis has recently emerged as a promising strategy for the degradation of organic contaminants in water and wastewater, according to several studies [17–19]. When semiconductors are exposed to light energy having energy greater than or equal to the band gap, electron-hole (e^-/h^+) pairs are generated in the conduction and valence band of the semiconductor. These (e^-/h^+) pairs lead to the redox reaction over the surface of the semiconducting photocatalyst, resulting in the generation of reactive species viz., hydroxyl radicals ($^{\cdot}OH$) and superoxide radicals ($^{\cdot}O_2^-$). The reactive species reacts with organic pollutants and degrade them into smaller, less toxic fragments; this process is dependent on the effective charge separation [20–22]. Nevertheless, effective charge separation can be achieved by doping, coupling, and supporting the semiconducting materials with other metals, such as metal oxides. Due to this (e^-/h^+) pairs recombination rate decreases, which results in enhancing the photocatalytic efficiency of the photocatalyst [23, 24].

Nanoparticles are ideal for use in heterogeneous photocatalysis due to their microscopic size. Nanocrystalline semiconductors have unique chemical and physical characteristics compared to bulk materials. There are several materials reported by many researchers in the literature that are used as photocatalysts, such as ZnO, TiO_2, and Bi_2O_3 etc [25]. Based on the above-mentioned literature, we aim to prepare CdS and Ni-CdS thin films for photocatalytic applications. Three distinct crystal structures are revealed by the properties of nanocrystalline cadmium sulfide (CdS), an II-VI semiconductor: cubic zinc mix, hexagonal wurtzite, and the high-pressure rock-salt phase [26, 27]. The hexagonal phase of CdS exhibits stability and is easily synthesized, while the cubic and rock-salt phases can be identified in nanocrystalline CdS. The variation in crystallization structures that arises from size reduction significantly influences the electronic properties of nanocrystalline materials. Due to its extensive band gap (E_g), CdS has garnered significant attention in research concerning its emission characteristics over a broad spectrum of wavelengths, encompassing from blue to red. It may be used as a window material in heterojunction solar cells and as an n-type material with other p-type materials in p-n junction solar cells. The conductivity type of CdS nanoparticles can be changed from n-type to p-type by doping them with different elements. These nanoparticles find application in a wide variety of photovoltaic devices, including electronic-powered lasers, photodetectors, LEDs, and field effect transistors. The fabrication of CdS nanoparticles has been accomplished using a variety of techniques, including chemical precipitation, hydrothermal procedures, laser ablation, photochemical methods, one-pot synthesis, and solvothermal processes [28–31]. Recent investigations are centered on altering the properties of CdS semiconductors via doping with rare earth and transition metals to augment its prospective applications. Several studies have explored the chemical synthesis of transition metal-doped CdS nanoparticles, analyzing the influence of dopants on the characteristics of CdS thin films [32]. This investigation seeks to enhance comprehension of the effects of doping on the behavior and performance of CdS thin films. Various methods have been employed to synthesize metal-doped CdS, including chemical precipitation, the hydrothermal process, chemical vapor deposition (CVD), and spray pyrolysis. The optical and electrical properties of metal-doped CdS, encompassing metals such as Ni, Co, Sb, and Ce, are garnering significant interest [33, 34]. This study employed the chemical bath deposition approach to prepare CdS and Ni-CdS thin films. The photocatalytic degradation of MB was investigated at neutral pH, and the effect of initial dye concentration and contact time was examined. The study reported enhanced photocatalytic property Ni-CdS thin for the MB dye as compared to the bare CdS thin film.

2. Experimental

2.1 Materials

Cadmium Sulphate [$CdSO_4 \cdot 8/3H_2O$], Nickel Sulphate [$NiSO_4.6H_2O$], Thiourea [CH_4N_2S], Triethanolamine (TEA), 30% Ammonia [NH_4OH], and Labolene with an analytical grade were purchased from Loba-Chemie and used without further purification.

2.2 Synthesis of CdS and Ni-doped CdS thin film

Thoroughly cleaning the substrate is essential for achieving uniform and impurity-free thin film deposition using the solution growth technique. Once the silica glass substrates have been cleaned with a mixture of chromic acid, deionized water, labolene detergent solution, and hot distilled water, they are put through an ultrasonic drying process. The CdS and Ni-doped CdS thin film was prepared by using a straightforward chemical solution deposition technique. Dissolve 0.09 M of $CdSO_4 \cdot 8/3\ H_2O$ and 0.09 M Thiourea in 50 mL of deionized water in two separate beakers. The 1% Ni-doping was achieved by adding 50 mL of 0.01 M [$NiSO_4.\ 6H_2O$] solution in deionized water into the $CdSO_4$ solution. Next, add an ammonia solution until the solution turns transparent, keeping the pH at approximately 11 while stirring continuously. Now, gradually add a few drops of

TEA to the Cadmium/Nickel sulphate solution. After that, steady stirring was used to incorporate the Thiourea solution into the Cadmium/Nickel sulfate solution. Glass surfaces that had already been cleaned were put vertically into the bath that was heated to $60-65$ °C for 70 minutes in a water bath. Consequently, this results in Ni-CdS thin films that are stable, adherent, and homogenous. The obtained Ni-CdS thin films were washed with deionized water and dried in the air environment. The same procedures were employed for the bare CdS thin film, avoiding the addition of a Nickel source into the CdS bath [35]. Fig. 1 represents the preparation of Ni-CdS thin by using the chemical bath deposition method.

2.3 Characterization techniques

The crystalline nature and purity of the fabricated Ni-doped CdS thin film were examined by using the X-ray diffraction (XRD) study (XRD- Bruker D 8 Advance X-Ray diffractometer Germany). The SEM Hitachi S-4800 Japan Instrument was used to analyze the morphology of the fabricated thin film. Elemental analysis was carried out by using electron dispersive X-ray spectroscopy (EDAX- Nova Nano SEM 450). The photocatalytic degradation experiment was performed by using a UV-visible, double-beam spectrophotometer (Systronics-2203).

2.4 Preparation of dye solution

A stock solution of MB (100 mg/L) was prepared with deionized water. The dye solutions at concentrations of 5, 10, and 15 mg/L were prepared through the dilution of the stock solution using deionized water.

2.5 Photocatalytic degradation experiment

The photocatalytic effectiveness of bare and Ni-doped CdS was tested for MB degradation under UV-visible light. Before measuring optical absorption, the bath with different MB solution concentrations was left in darkness for 30 minutes to create adsorption-desorption equilibrium. The beakers were illuminated within a photocatalytic reactor using a 160 W mercury vapor lamp from the Mumbai-based Lelesil Innovative System after 30 minutes. Using MB concentrations between 5 and 15 mg/L, the degradation process began at time t = 0 and proceeded for the next 90 minutes. We collected enough samples at a certain time and spun them in a centrifuge for five minutes to get rid of any suspended particles. An ultraviolet-visible double beam spectrophotometer was used to examine the supernatant at the absorbance maximum wavelength (MB max = 664 nm) in order to determine the concentration of MB in the solution. Equation (1) was used to determine the dye degradation [36].

$$\text{Degradation} = \frac{(C_0 - C_t)}{C_0} \times 100 \qquad (1)$$

where C_0 is the initial dye concentration, and C_t is the dye concentration after time t.

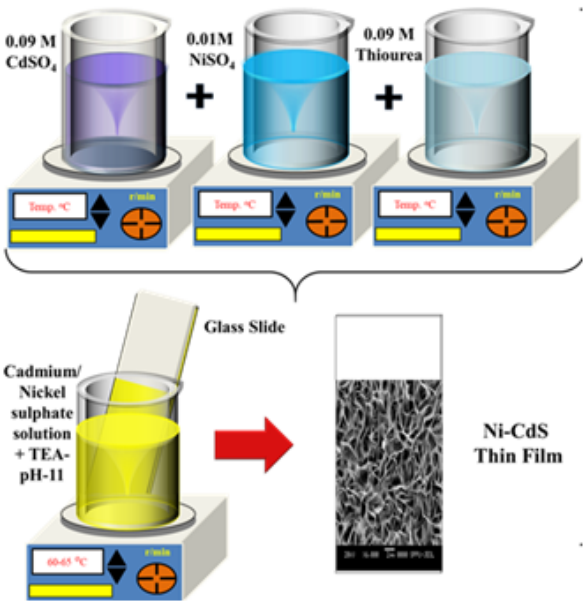

Figure 1. Schematic representation of preparation of Ni-CdS thin film.

3. Results and discussion

3.1 X-Ray diffraction analysis

Fig. 2a. Shows the X-ray diffraction patterns of the CdS and Ni-CdS thin films. The peaks at $2\theta = 26.48°$, 29.3°, 31.04°, and 51.3° in the diffraction pattern represent the distinctive peaks of pure CdS, whereas the peaks at $2\theta = 26.3°$, 28.8°, 29.2°, 30.9°, and 51.2° belong to the Ni-CdS thin film. The fact that the diffraction pattern of Ni-CdS is somewhat different from that of pure CdS suggests that the crystalline phase remains unchanged. The reflection of the (002), (101),

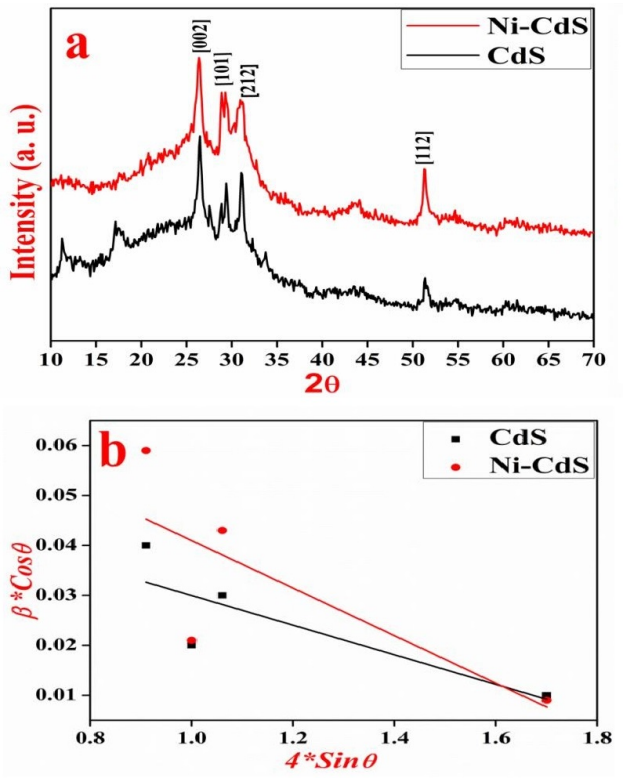

Figure 2. (a) XRD pattern of CdS and Ni-CdS thin film (b) Williamson-Hall plot of CdS and Ni-CdS thin film.

Table 1. The lattice parameters of CdS and Ni-doped CdS thin film.

Thin Film	2θ	FWHM (β)	Average Crystallite Size by Scherrer Formula	Average Crystallite Size by Williamson-Hall Method
CdS	26.48	2.9	4.26	2.3
	29.3	1.7		
	31.04	1.8		
	51.3	0.75		
Ni-CdS	26.3	3.5	3.70	1.5
	28.8	3.5		
	29.2	1.3		
	30.9	2.6		

(212), and (112) dhkl planes may be attributed to the strong peaks of the diffraction pattern, which is in good accord with JCPDS card numbers $01-0780$ and $89-2944$ [37]. The outcome shows that the CdS and Ni-CdS thin films have a hexagonal structure along the (101) crystallite orientation. In addition to functioning as a substitutional impurity, the Ni^{2+} dopant can occupy interstitial lattice positions. However, Cd^{2+} has an ionic radius of 97 pm, while Ni^{2+} has an ionic radius of 78 pm. To avoid acting as a surface contaminant, Ni^{2+} can instead occupy interstitial sites due to its lower ionic radius compared to Cd^{2+} [38]. Applying the Scherrer formula, the observed crystallite sizes of the CdS and Ni-CdS thin films were found to be 4.26 nm and 3.70 nm, respectively. The crystallite size of both thin films was estimated using the Williamson-Hall equation (4).

$$\beta\cos\theta = \varepsilon(4\sin\theta) + \frac{K\lambda}{D} \tag{2}$$

where β is the full width at half maximum in radians of the diffraction peak being considered after instrumental broadening correction, θ is the angle of diffraction, D is the size of the crystallite, and ε is the strain in the material. Figure 2b shows the plot of $\beta\cos\theta V_s 4\sin\theta$. Table 1 displays the results of directly calculating the average crystallite size D from the Y-intercept for each sample. Crystallite sizes for CdS were found to be 2.3 nm and for Ni-CdS thin film to be 1.5 nm, which is by the sizes predicted by the Scherrer equation and reported in Table 1 [39, 40].

3.2 Scanning electron microscopy

The scanning electron micrographs of the pure CdS thin film show a densely packed uniform porous structure and well-adherent deposition over the entire substrate. The surface has an increased surface area due to its porous structure, which is marked by separate pores of different sizes. As seen in figure 3(a, b), the nanoflakes are interconnected to each other, resulting in the formation of an irregularly developed nanosheet-like morphology that is uniformly distributed over the surface of the thin film. Compared to the undoped CdS, the scanning electron micrographs of the nickel-doped CdS thin film show much better-grown nanosheet-like morphology formed by the regular arrangement of smaller interconnected nanoflakes, as seen in figure 3(c, d). The alternation in the morphology from irregularly developed nanosheets to well-developed nanosheets-like morphology with enhanced surface area for scattering and absorption of light. The Ni ions incorporated into the CdS crystal lattice may be responsible for the evolution of sheets like nanoflakes, which minimize surface energy, accumulate randomly moving CdS monomers, and then self-organize [41, 42]. Such morphological shift can enhance photocatalytic performance by increasing roughness and porosity, which in turn promote charge carrier separation and light absorption. The nickel-doped CdS thin film shows great promise for photocatalytic improvements because of its uniformly developed nanosheet-like morphology. There may be more adsorption sites accessible for dye molecules due to the larger surface area and the presence of smaller pores,

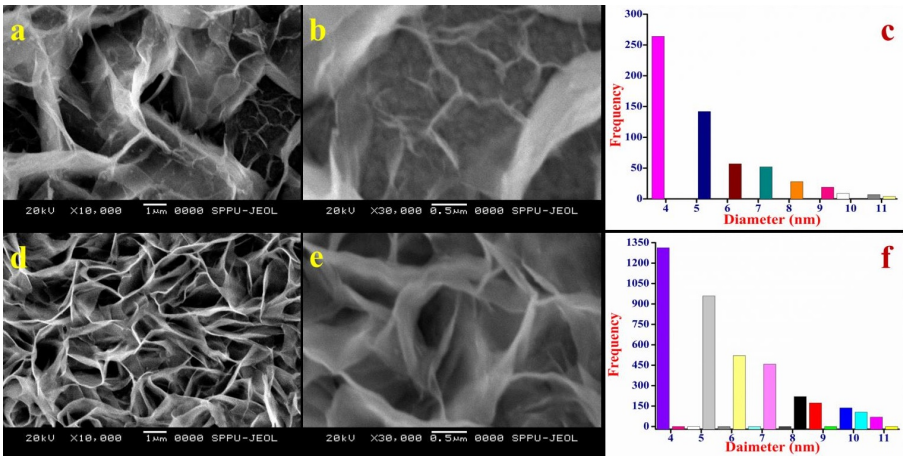

Figure 3. SEM images of CdS (a, b), Ni-doped CdS thin film (c, d), and particle size distribution of CdS (c), Ni-CdS (f).

which might improve degradation efficiency. Figures 3c and f indicate that the average crystallite size, as determined by the Scherrer formula, is close to the particle size distribution derived from scanning electron microscopy images of CdS and Ni-CdS thin films [43, 44].

3.3 Energy dispersive X-ray spectroscopy (EDXS) analysis

Figure 4 illustrates that the expected elements were verified by the EDXS spectra of the doped materials, which exhibited distinct peaks for Cd, S, and Ni. The EDX spectra of the undoped CdS thin film indicated that the primary constituents were cadmium (Cd) and sulphur (S). According to the atomic ratio, the CdS stoichiometric composition is in agreement with the Cd/S ratio. The EDX spectra of the Ni-doped CdS thin film showed distinct peaks for Cd, S, and Ni. The presence of an EDX signal indicative of Ni confirmed its integration into the CdS lattice. Ni atomic percentage in the doped sample was close to 1%, which was in line with the desired concentration of doping. The atomic ratio of Cd to S was nearly the same as in the undoped sample, indicating that the doping method did not significantly alter the stoichiometry of the CdS matrix. The flawless sample proved that the manufactured film was of the highest quality [45].

3.4 UV-Visible diffuse reflectance spectroscopy

Essential for their photocatalytic applications, the optical properties and band gap energies of the synthesized CdS and nickel-doped CdS thin films were investigated using UV-visible diffuse reflectance spectroscopy (UV-DRS). In the UV-DRS spectra, the characteristic visible absorption edge of CdS is evident in the thin film of pure CdS. There is a correlation between the absorption edge and the direct band gap transition. The obtained reflectance was applied to the Kubelka-Munc equation and Tauc's plot, and extending the linear portion of figure 5, it was feasible to determine that the optical band gap of the CdS and Ni-CdS thin film was about 2.29 and 2.03 eV respectively [46, 47]. The known band gap of CdS is commensurate with this value, making it perfect for visible-light-driven photocatalysis. In the UV-DRS spectra, a redshift is seen when comparing the absorption edge of the pure CdS film with that of the nickel-doped CdS thin film. The addition of nickel to the CdS lattice explains this alteration, which implies a reduction in the band gap energy. There are significant implications for photocatalytic applications stemming from the material's ability to absorb a broader spectrum of visible light, made possible by the nickel doping-induced reduction in band gap energy. Dye degradation efficiency is dependent on the ability to produce an adequate number of electron-hole pairs when exposed to visible light; a smaller band gap facilitates this process [48, 49].

Further, the potential position of V_B and C_B of CdS and Ni-CdS thin film was calculated by using the empirical formula as shown in equation (3).

$$E_{\mathrm{VB}} = X - E_e + 0.5E_g \tag{3}$$

where X absolute electronegativity of the material (eV), which is the geometric mean of the electronegativities of the constituent atoms, E_e energy of free electrons on the hydrogen scale, approximately 4.5 eV and Band gap energy of the semiconductor (eV). The absolute electronegativity (X) of the used semiconductor can be evaluated by half value of summation of the first ionization energy (E_i) and electron affinity (E_a) of the corresponding elements, and the results are tabulated in Table 2. The potential position of V_B was estimated using the above-mentioned formula and used to estimate the potential position of C_B by using the empirical relation of V_B and C_B as $E_{\mathrm{CB}} = E_{\mathrm{VB}} - E_g$. All

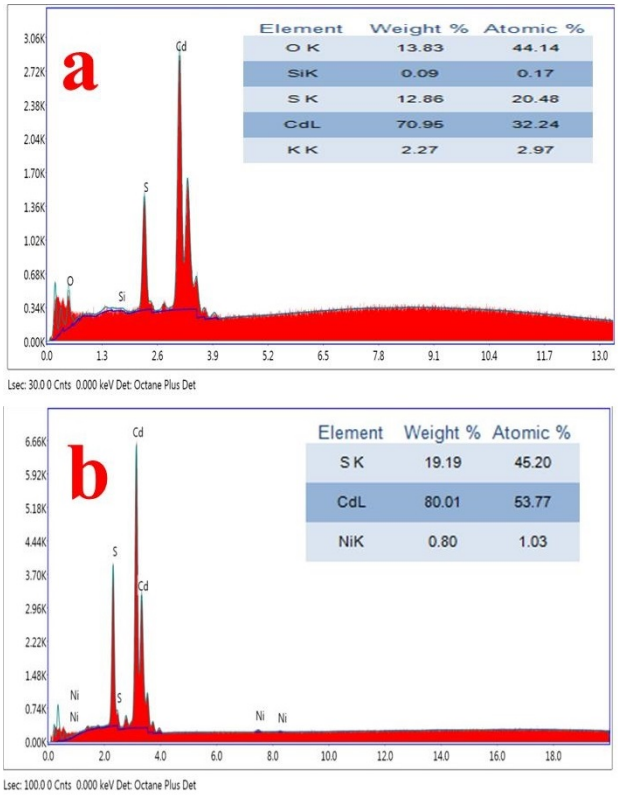

Figure 4. EDAX spectra of CdS (a) and Ni-doped CdS thin film (b).

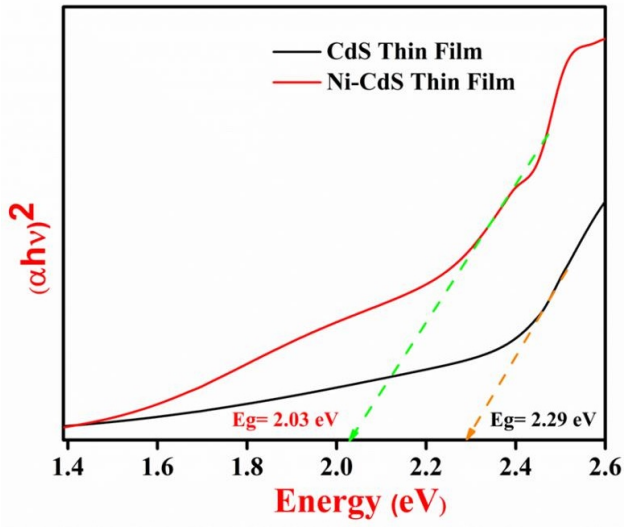

Figure 5. Tauc's plot of CdS and Ni-doped CdS thin film.

Table 2. Mulliken electronegativity of the constituent elements of the CdS and Ni-CdS thin films by using their electron affinity (E_a) and the first ionization energy (E_i) in eV.

Element	E_a (eV)	E_i (eV)	$(E_a+E_i)^{1/2}$ (eV)
Cadmium (Cd)	−0.7	8.994	2.764
Sulphur (S)	2.077	10.360	4.145
Nickel (Ni)	1.157	7.639	2.932

the results are summarised in Table 3. The results of the potential position calculation were used to draw a schematic energy level diagram to explain the charge transfer in the CdS and Ni-CdS thin films [50–52].

3.5 Photocatalytic degradation of methylene blue dye

3.5.1 Effect of initial dye concentration

Both the degradation rate and the total efficiency are affected by the initial concentration of MB, which is a key component in photocatalytic degradation. Various initial concentrations of MB dye, ranging from 5 mg/L to 15 mg/L, were tested using pure CdS and Ni-doped CdS thin films, as shown in Fig. 6(a-b). Degradation efficiency decreased linearly with increasing starting MB concentration from 5 mg/L to 15 mg/L. After 120 minutes at a lower dosage of 5 mg/L, the degradation efficiency reached around 69%, indicating stronger photocatalytic activity. In contrast, at 15 mg/L concentration, the efficiency decreased to about 56%. This is because as the concentration goes up, the active sites on the CdS thin film surface fill up with dye molecules. This makes them less available for photon absorption and lowers the number of reactive species that are made. In comparison to pure CdS thin film, the Ni-doped CdS thin film demonstrated superior photocatalytic activity across all concentrations. Once exposed to light for 120 minutes, the degradation efficiency increased to 84% from 5 mg/L starting concentration of MB. Even though the efficiency dropped to 54% at 15 mg/L, it was still better than pure CdS [53, 54].

Nickel, when added to a CdS matrix, slows down electron-hole recombination and enhances charge separation. More reactive species become accessible for degradation as a result of this. The results indicate that the degrading performance is greatly enhanced by Ni-doping, particularly at higher dye concentrations. This study concludes that Ni-doped CdS thin films may enhance photocatalytic destruction of organic pollutants. Results demonstrate that when exposed to visible light, Ni-doped CdS thin films outperform pure CdS films in terms of photocatalytic activity. The degradation rate is improved by doping and remains quicker with increasing dye concentration and increasing contact length. The breakdown of MB dye is mainly caused

Table 3. Band gap energies and potential positions of V_B and C_B of the CdS and Ni-CdS thin film.

Catalyst	X (eV)	E_g (eV)	V_B (eV)	C_B (eV)
CdS	12.895	2.29	9.540	7.250
Ni-CdS	11.204	2.03	7.719	5.689

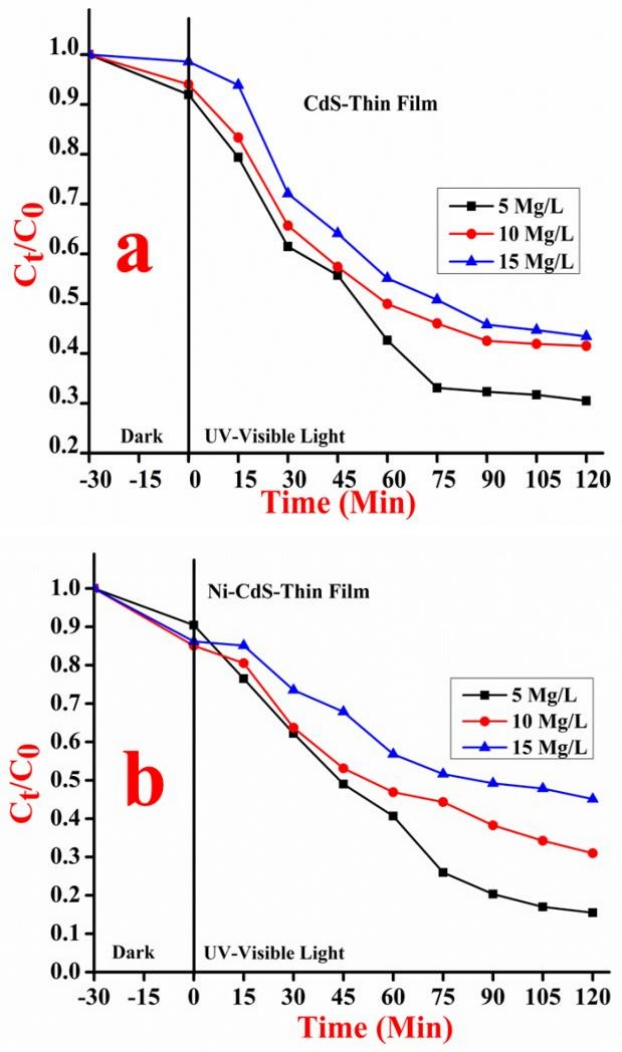

Figure 6. (a-b) Effect of initial dye concentration on the photocatalytic degradation of MB by CdS and Ni-CdS thin film: Conditions pH = 7, dye concentration 5, 10, 15 mg/L, and for irradiation time 120 min.

by reactive species such as hydroxyl radicals (·OH) and superoxide anions (O_2^-), which are made more readily available when nickel is doped into CdS, which improves the separation of photo-generated electron-hole pairs [55–58].

3.6 Effect of contact time

The photocatalytic degradation process is also greatly affected by the contact time. For 150 minutes, the MB degradation of CdS and Ni-CdS thin films was tracked at regular intervals to examine the impact of contact time. MB degradation for CdS thin films increased somewhat with increasing contact time. At a dye concentration of 5 mg/L, the degradation efficiency peaked at 75% after 150 minutes, having reached 58% after 75 minutes. Degradation slowed dramatically after 90 minutes, which could be because the thin film surface had used up all of its active sites, and the solution contained fewer dye molecules [38, 59]. The thin sheet of CdS doped with Ni deteriorated at a quicker pace. Degradation efficiency peaked at 71% after 75 minutes, and at 5 mg/L, 87% degradation was attained after the 150-minute illumination period, as shown in Fig. 7.

Faster formation of reactive oxygen species and degradation

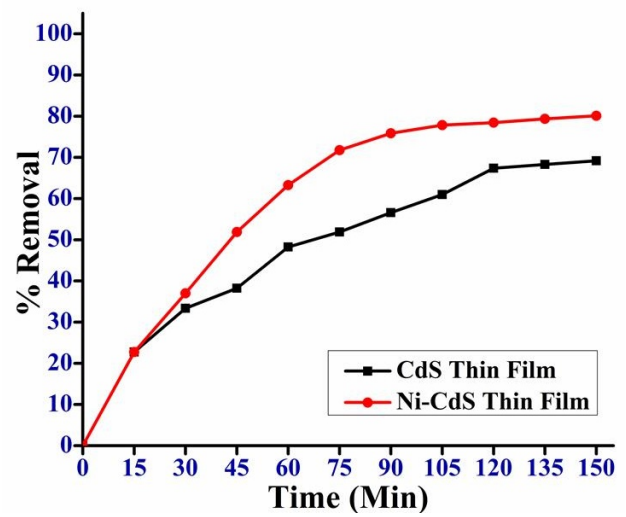

Figure 7. Effect of contact time on photocatalytic degradation of MB by CdS and Ni-CdS thin film: Conditions pH = 7, dye concentration 5 mg/L, and for irradiation time 150 min.

of the dye molecules are the outcomes of better charge transfer dynamics in Ni-doped CdS film, which is responsible for the increased performance. Degradation rates were also more maintained in the Ni-doped films, even after 90 minutes, suggesting that these films made better use of surface sites and had reactive species that lasted longer [60].

3.7 Kinetic study

A kinetic analysis was carried out to gain a better understanding of the photocatalytic degradation mechanism of MB employing CdS and Ni-CdS thin films. According to the Langmuir-Hinshelwood model, as seen in figure 8(a-b), the degradation of MB when exposed to visible light follows pseudo-first-order kinetics. The degradation rate is assumed to be directly proportional to the concentration of the remaining dye in this model. Here is equation (4), which represents the photocatalytic degradation process kinetics.

$$\ln \frac{C_0}{C_t} = kt \tag{4}$$

where C_0 is the initial concentration of MB (mg/L), C_t is the concentration of MB at time t, k is the apparent rate constant (min^{-1}), and t is the time (minutes). By plotting ln (C_0/C_t) versus time, the rate constant k was determined from the slope of the linear plot. The pseudo-first-order kinetics of the process were confirmed by the linear connection between $\ln(C_0/C)$ and time seen in the degradation of MB utilizing the CdS and Ni-CdS thin films. Table 4 summarizes the findings of calculating the apparent rate constants k for different beginning concentrations of MB. Kinetic analysis demonstrates that CdS and Ni-doped CdS

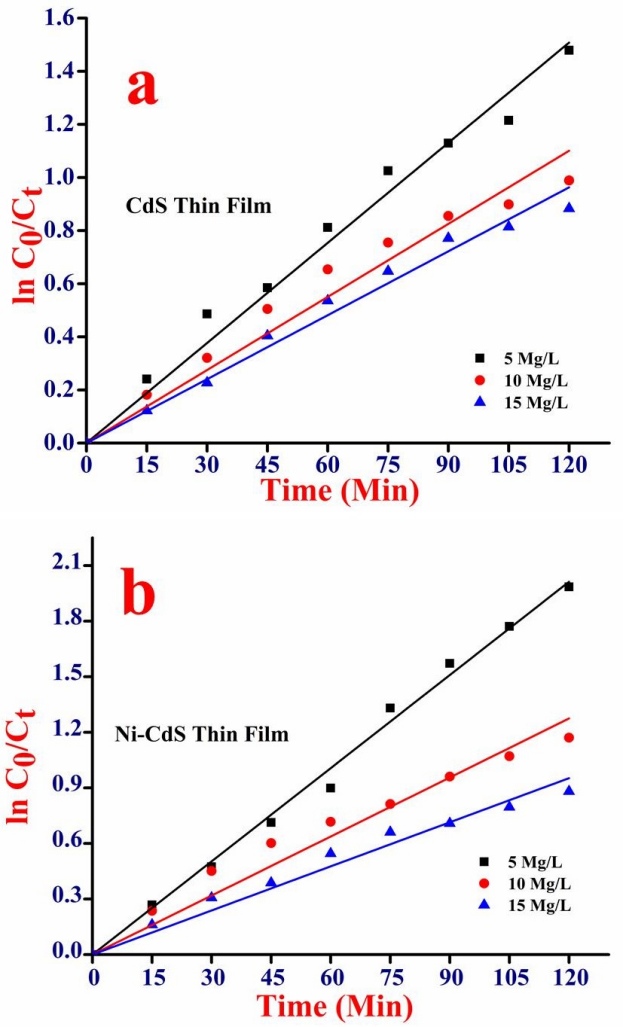

Figure 8. (a-b) Pseudo first-order kinetics for photocatalytic degradation of MB by CdS and Ni-CdS thin film: Conditions pH = 7, dye concentration. 5, 10, 15 mg/L and irradiation time 120 min.

thin films degrade MB photocatalytically according to pseudo-first-order kinetics. The degradation rate is dramatically improved by Ni-doping, which lowers the activation energy and increases the rate constant. Improved charge separation, higher surface activity, and wider light absorption are the reasons why Ni-doped CdS thin films work better. The results show that Ni-doped CdS thin films could be used as effective photocatalysts for treating wastewater [61–65].

3.8 Reusability experiment

Synthesized CdS and Ni-doped CdS thin film was investigated for MB elimination by photocatalytic degradation cycles. After the first cycle, the films were carefully cleaned

Table 4. The pseudo first-order rate constant of MB photocatalytic degradation.

Amount of Catalyst (g/mL)	Concentration of dye (g/mL)	Rate Const. (K) min^{-1}		Linear regression coefficient (R^2)	
		CdS	Ni-CdS	CdS	Ni-CdS
1	5	0.0287	0.0384	0.994	0.997
1	10	0.0211	0.0244	0.986	0.987
1	15	0.0184	0.0182	0.997	0.991

with water and ethanol numerous times and dried in an open-air oven at 120 °C for 1 hr. In order to photocatalytically degrade MB using CdS and Ni-doped CdS films, these three catalytic cycles were performed. The film's reusability over numerous cycles was proven by this. Figure 9(a-b) shows that up to the third cycle, there is a little drop in adsorption and a 22% drop in catalytic efficiency for MB for CdS and a 20% drop for Ni-doped CdS, respectively. This implies that for the degradation of organic pollutants, the thin films are quite stable and effective [66].

3.9 Possible degradation pathway

Figure 10 shows the possible degradation mechanism of the MB dye degradation in the presence of CdS and Ni-CdS thin films. For the reduction of O_2 into the $\cdot O_2^-$, the CB must be more negative than the reduction potential of $O_2/\cdot O_2^-$ (-0.33 eV). In the case of CdS thin film, the CB ($+5.68$ eV) is more positive; therefore, the electron in CB doesn't have sufficient energy potential to reduce molecular O_2 into the superoxide radicals. As a result, the generation of superoxide radicals would be significantly suppressed. While the generation of hydroxyl radicals ($\cdot$OH), the VB must be more positive than the oxidation potential of $^-$OH/$\cdot$OH ($+2.38$ eV). However, the VB ($+7.71$ eV) of CdS is more positive, which indicates that the holes (h^+) in VB have enough energy to oxidize the $^-$OH/H_2O molecule into the $\cdot$OH radicals. These $\cdot$OH radicals are highly reactive species that can degrade the organic dyes, i.e. MB.

When Ni^{2+} is incorporated into the crystal lattice of CdS thin film, then the new band positions are available to the charge transfer mechanism. The CB of Ni^{2+} (-1.1 eV) is now significantly more negative than the $O_2/\cdot O_2^-$; this enables the reduction of oxygen molecules into the superoxide radicals ($\cdot O_2^-$), an important reactive oxygen species (ROS) for the degradation process. Also, the VB of Ni^{2+} ($+2.5$ eV) is more positive than the oxidation potential of $^-$OH/$\cdot$OH, maintaining the ability to oxidize $^-$OH/H_2O molecule into the $\cdot$OH radicals. Therefore, Ni^{2+} doping introduces the mid-gap states electronic structure, reducing the e^-/h^+ recombination. However, the broader energy window between the VB and CB of Ni-CdS thin film enhances the potential for dual ROS pathways, such as reductive and oxidative pathways [67].

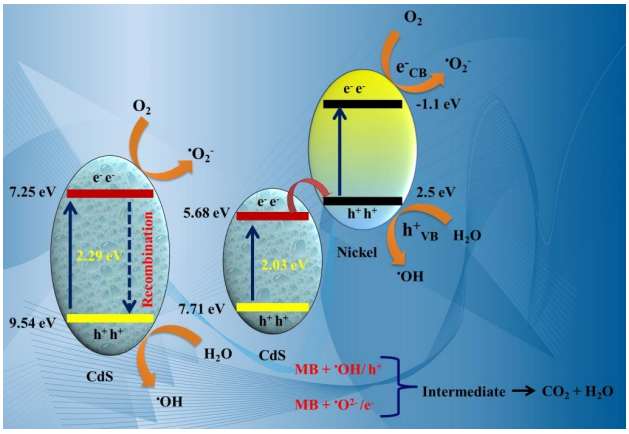

Figure 10. Schematic representing the possible degradation mechanism of MB using CdS and Ni-CdS thin film.

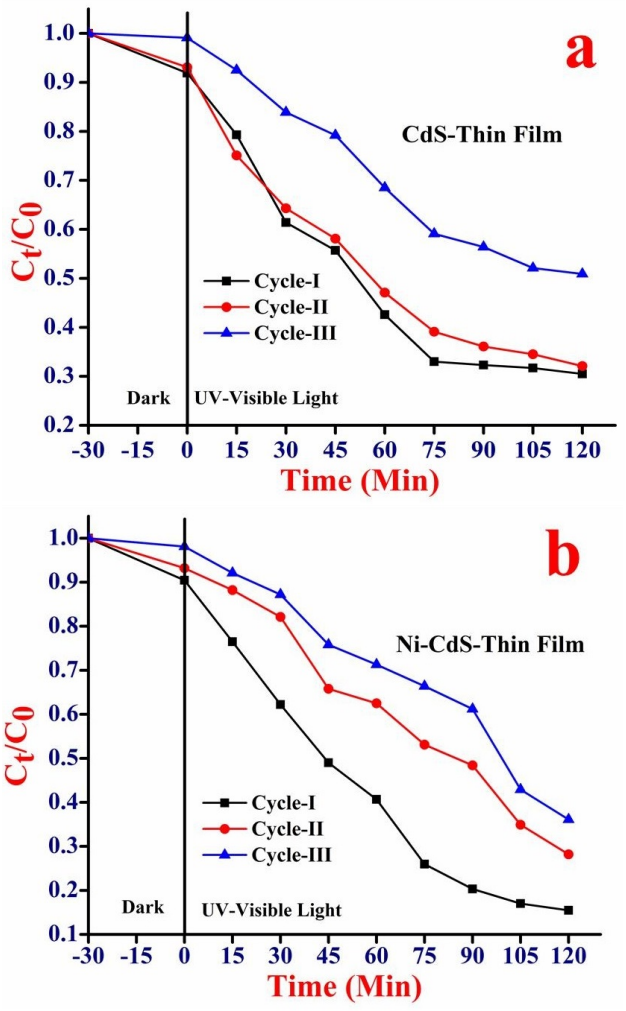

Figure 9. Reusability experiment for the photocatalytic degradation of MB by CdS (a) and Ni-CdS (b) thin films.

3.10 Comparison

Table 5 shows a comparison of the photocatalytic degradation of MB with different photocatalysts. This includes

Table 5. Comparison of photocatalytic degradation of MB dye with reported literature.

Sr. No.	Photocatalyst	Reaction time (min)	% Degradation	Reference
1	NiO-CdS nanoparticles	83	80	[29]
2	CdS-AgBr nanocomposite	60	98	[55]
3	CdS/Ag_3PO_4 nanoparticles	139	85	[57]
4	CdS Thin Film	60	80	[68]
5	Ni-CdS Thin Film	120	84	This Study

multiple reports featuring photocatalysts in powder form [29, 55, 57]. This study reveals findings regarding the degradation of MB using the 2D form of CdS and Ni-doped CdS. The percentage of degradation of MB observed with Ni-CdS in this instance aligns closely with the reports referenced. The 2D form of Ni-CdS demonstrates significant potential as a substitute for traditional photocatalysts. The thin films provide better stability and a controlled surface area, which minimizes aggregation and boosts catalytic efficiency.

4. Conclusion

The CdS and Ni-CdS thin films were prepared using the simple chemical bath deposition technique. The hexagonal structure along the (101) crystallite orientation is revealed by the X-ray diffraction data of the CdS and Ni-CdS thin films. The morphological examination of CdS and Ni-CdS thin films reveals alternation in the morphology from irregularly developed nanosheets to well-developed nanosheets-like morphology with enhanced surface area for scattering and absorption of light, which facilitates effective charge separation. UV-DRS measurement of Ni-CdS thin films clearly shows a redshift, indicating a reduction in band gap energy due to nickel incorporation into CdS crystal lattices. The CdS and Ni-CdS thin film demonstrates remarkable photocatalytic degradation of MB dye when exposed to visible light irradiation. The photocatalytic degradation of a 5 mg/L concentration of MB was observed to reach 69% and 84% using CdS and Ni-CdS thin films over 120 minutes, respectively. It has been found that Ni^{2+} incorporation into the CdS matrix, which provides the new band gap position of VB and CB for the Ni-CdS thin film, leads to the generation of dual ROS pathway. The photocatalytic investigation follows pseudo-first-order kinetics, exhibiting a strong association with the linear regression coefficient.

Acknowledgement:
RSP and VSS thankful to DST-FIST for providing the necessary instruments in a research laboratory. RSP is grateful to the Management and Principal, NTVS's G.T. Patil College Nandurbar for encouragement and support. The authors are thankful to the UGC-DAE consortium for scientific research, Indore, Department of Physics, SPPU, Pune, and SICART Vallabh Vidya Nagar, Gujarat for characterization facilities.

Authors contributions
Authors were contributed equally to perform the experiment and preparing the paper.

Availability of data and materials
The data that could support our findings are available in the text of this article.

Conflict of interests
On behalf of all authors, the corresponding author states that there is no conflict of interest.

References

[1] M. E. Awual, M. S. Salman, M. M. Hasan, M. N. Hasan, K. T. Kubra, M. C. Sheikh, A. I. Rasee, A. I. Rehan, R. M. Waliullah, M. S. Hossain, H. M. Marwani, A. M. Asiri, M. M. Rahman, A. Islam, Khaleque M. A., and M. R. Awual. *Ind. Eng. Chem.*, **131**(2024): 585–592.
DOI: https://doi.org/10.1016/j.jiec.2023.10.062.

[2] M. S. Hossain, M. A. Shenashen, M. E. Awual, A. I. Rehan, A. I. Rasee, R. M. Waliullah, K. T. Kubra, M. S. Salman, M. C. Sheikh, et al. *PSEP*, **185**(2024):367–374.
DOI: https://doi.org/10.1016/j.psep.2024.03.026.

[3] S. Ghattavi and A. Nezamzadeh-Ejhieh. *Compos. B Eng.*, **183**(2020): 107712, .
DOI: https://doi.org/10.1016/j.compositesb.2019.107712.

[4] H. Derikvandi and A. Nezamzadeh-Ejhieh. *Solid State Sci.*, **101**(2020):106127.
DOI: https://doi.org/10.1016/j.solidstatesciences.2020.106127.

[5] M. Rezaei, Nezamzadeh-Ejhieh A., and A. R. Massah. *ACS Omega*, **9(6)**(2024):6093–6127, .
DOI: https://doi.org/10.1021/acsomega.3c07560.

[6] G. Gunawan, N. B. A. Prasetya, Widodo D. S., and R. A. Wijaya. *KIJOMS*, **9(4)**(2023):725–741.
DOI: https://doi.org/10.33640/2405-609X.3333.

[7] A. Gupta and R. Gupta. *Adv. Biol. Treat. Ind. Wastewater Recycl. Sustain. Future*, (2019):13–49.
DOI: https://doi.org/10.1007/978-981-13-1468-1-2.

[8] A. Kumar, Singh A. K., and R. Chandra. *Emerg. Treat. Technol. Waste Manag*, (2021):1–28.
DOI: https://doi.org/10.1007/978-981-16-2015-7-1.

[9] M. Abedi, G. Mahmoudi, P. Hayati, B. Machura, F. I. Zubkov, K. Mohammadi, S. Bahrami, H. Derikvandi, Mehrabadi Z., and A. M. Kirillov. *New J. Chem.*, **43(44)**(2019):17457–17465.
DOI: https://doi.org/10.1039/C9NJ04382A.

[10] M. R. Awual. *Chem. Eng. J.*, **266**(2015):368–375, .
DOI: https://doi.org/10.1016/j.cej.2014.12.094.

[11] M. R. Awual. *Chem. Eng. J.*, **307**(2017):85–94, .
DOI: https://doi.org/10.1016/j.cej.2016.07.110.

[12] T. Islam, M. R. Repon, T. Islam, Sarwar Z., and M. M. Rahman. *Environ. Sci. Pollut. Res.*, **30(4)**(2023):9207–9242.
DOI: https://doi.org/10.1007/s11356-022-24398-3.

[13] D. Patel and S. Bhatt. *Biotechnol. Genet. Eng. Rev.*, **38(1)**(2022): 33–86.
DOI: https://doi.org/10.1080/02648725.2022.2048434.

[14] M. E. Nedu, M. Tertis, Cristea C., and A. V. Georgescu. *Diagnostics (Basel)*, **10**(2020):223.
DOI: https://doi.org/10.3390/diagnostics10040223.

[15] H. Dabhane, S. Ghotekar, P. Tambade, S. Pansambal, H. C. A. Murthy, Oza R., and V. Medhane. *Environ. Chem. Ecotoxicol.*, **3**(2021):209–219.
DOI: https://doi.org/10.1016/j.enceco.2021.06.002.

[16] R. Singh, D. Pal, A. Mathur, A. Singh, Krishnan M. A., and S. Chattopadhyay. *React. Funct. Polym.*, **144**(2019):104346.
DOI: https://doi.org/10.1016/j.reactfunctpolym.2019.104346.

[17] Z. H. Jabbar and S. Esmail Ebrahim. *J. Environ. Nanotechnol. Monit. Manag.*, **17**(2022):100666.
DOI: https://doi.org/10.1016/j.enmm.2022.100666.

[18] A. G. Akerdi and S. H. Bahrami. *J. Environ. Chem. Eng.*, **7(5)**(2019): 103283.
DOI: https://doi.org/10.1016/j.jece.2019.103283.

[19] A. Majid and M. Bibi. *Gewerbestrasse*, **11**(2018):6330.
DOI: https://doi.org/10.1007/978-3-319-68753-7.

[20] A. Yousefi and A. Nezamzadeh-Ejhieh. *Iran. J. Catal.*, **11(3)**(2021): 247–259.

[21] M. Rezaei and A. Nezamzadeh-Ejhieha. *Int. J. Hydrogen Energy*, **45(46)**(2020):24749–24764.
DOI: https://doi.org/10.1016/j.ijhydene.2020.06.258.

[22] M. Rezaei, A. Nezamzadeh-Ejhieha, and A. R. Massah. *Energy Fuels*, **38(10)**(2024):8406–8436, .
DOI: https://doi.org/10.1021/acs.energyfuels.4c00160.

[23] Z. Mehrabadi, H. Faghihian, and J. Photochem. *Photobiol. A: Chem.*, **356**(2018):102–111.
DOI: https://doi.org/10.1016/j.jphotochem.2017.12.042.

[24] M. R. Awual. *J. Environ. Chem. Eng.*, **7(5)**(2019):103378, .
DOI: https://doi.org/10.1016/j.jece.2019.103378.

[25] T. Tamiji and A. Nezamzadeh-Ejhieh. *Solid State Sci.*, **98**(2019): 106033.
DOI: https://doi.org/10.1016/j.solidstatesciences.2019.106033.

[26] T. Ahamad, M. A. Majeed Khan, S. Kumar, M. Ahamed, Shahabuddin M., and A. N. Alhazaa. *J. Appl. Phys. B*, **122(6)**(2016):179.
DOI: https://doi.org/10.1007/s00340-016-6455-3.

[27] I. M. Dharmadasa and A. A. Ojo. *J. Mater. Sci.: Mater. Electron*, **28(22)**(2017):16598–16617.
DOI: https://doi.org/10.1007/s10854-017-7615-x.

[28] T. Sinha, D. Lilhare, and A. Khare. *J. Mater. Sci.*, **45(19)**(2019): 12189–12205.
DOI: https://doi.org/10.1007/s10853-019-03651-0.

[29] S. Senobari and A. Nezamzadeh-Ejhieh. *J. Mol. Liq.*, **257**(2018): 173–183.
DOI: https://doi.org/10.1016/j.molliq.2018.02.096.

[30] K. Hachem, M. J. Ansari, R. O. Saleh, H. H. Kzar, M. E. Al-Gazally, U. S. Altimari, S. A. Hussein, H. T. Mohammed, Hammid A. T., and E. Kianfar. *J. BioNanoScience*, **12(3)**(2022):1032–1057.
DOI: https://doi.org/10.1007/s12668-022-00996-w.

[31] M. H. Ullah and C. S. Ha. *J. Nanosci. Nanotechnol*, **5(9)**(2005): 1376–1394.
DOI: https://doi.org/10.1166/jnn.2005.309.

[32] D. Singhwal and P. S. Rana. *Water Air Soil Pollut*, **235(7)**(2024): 437.
DOI: https://doi.org/10.1007/s11270-024-07236-9.

[33] H. Yahi, C. Bourouis, and A. Meddour. *J. Superconduct*, **33(7)**(2020): 1917–1926.
DOI: https://doi.org/10.1007/s10948-020-05505-2.

[34] D. Zhu and Q. Zhou. *J. Environ. Nanotechnol. Monit. Manag.*, **12**(2019):100255.
DOI: https://doi.org/10.1016/j.enmm.2019.100255.

[35] A. Mukherjee, M. R. Das, A. Banerjee, and P. Mitra. *Thin Solid Films*, **704**(2020):138005.
DOI: https://doi.org/10.1016/j.tsf.2020.138005.

[36] S. D. Khairnar, M. R. Patil, and V. S. Shrivastava. *Iran. J. Catal*, **8(2)**(2018):143–150, .

[37] J. Yuvaloshini and R. Shanmugavadivu. *J. Mater. Sci.: Mater. Electron*, **27(9)**(2016):9379–9383.
DOI: https://doi.org/10.1007/s10854-016-4980-9.

[38] M. Sankar, M. Jothibas, A. Muthuvel, A. Rajeshwari, and S. J. Jeyakumar. *J. Surf. Interfaces*, **21**(2020):100775.
DOI: https://doi.org/10.1016/j.surfin.2020.100775.

[39] W. T. Salam, M. Ikram, I. Shahzadi, M. Imran, M. Junaid, M. Aqeel, S. Anjum, A. Shahzadi, Afzal H., and U. Sattar. *J. Nanoscience Nanotechnol. Lett*, **10(12)**(2018):1662–1670.
DOI: https://doi.org/10.1166/nnl.2018.2839.

[40] S. Vahabirad, A. Nezamzadeh-Ejhieh, and M. Mirmohammadi. *J. Taiwan Inst. Chem. Eng.*, **151**(2023):105139.
DOI: https://doi.org/10.1016/j.jtice.2023.105139.

[41] K. V. Khot, S. S. Mali, R. R. Kharade, R. M. Mane, P. S. Patil, C. K. Hong, J. H. Kim, J. Heo, and P. N. Bhosale. *J. Mater. Sci. Mater. Electron*, **25(12)**(2014):5606–5617.
DOI: https://doi.org/10.1007/s10854-014-2350-z.

[42] K. H. Aboud, S. Mh Al-Jawad, and N. Jamal Imran. *J. Nanostruct*, **12(2)**(2022):316–329.
DOI: https://doi.org/10.22052/JNS.2022.02.009.

[43] H. Zhang, Y. Wan, J. Luo, and S. B. Darling. *ACS Appl. Mater. Interfaces*, **13(13)**(2021):14844–14865.
DOI: https://doi.org/10.1021/acsami.1c01131.

[44] N. A. Marfur, N. F. Jaafar, M. Khairuddean, and N. Nordin. *Acta Chim. Slov*, **67(2)**(2020):361–374.
DOI: https://doi.org/10.17344/acsi.2019.5161.

[45] N. H. Patel, M. P. Deshpande, and S. H. Chaki. *J. Mater. Sci. Semicond. Process*, **31**(2015):272–280.
DOI: https://doi.org/10.1016/j.mssp.2014.11.039.

[46] A. Natarajan, M. Shanmuganathan, E. Jayabal, and V. Rangarajan. *Int. J. Nanotechnol*, **18(5-8)**(2021):400–413.
DOI: https://doi.org/10.1504/IJNT.2021.116161.

[47] N. Omrani and A. Nezamzadeh-Ejhieh. *J. Mol. Liq.*, **315**(2020): 113701.
DOI: https://doi.org/10.1016/j.molliq.2020.113701.

[48] A. Rmili, F. Ouachtari, A. Bouaoud, A. Louardi, T. Chtouki, B. Elidrissi, and H. Erguig. *J. Alloys Compd.*, **557**(2013):53–59.
DOI: https://doi.org/10.1016/j.jallcom.2012.12.136.

[49] M. Al Kausor and D. Chakrabortty. *Inorg. Chem. Commun*, **129**(2021):108630.
DOI: https://doi.org/10.1016/j.inoche.2021.108630.

[50] S. Ghattavi and A. Nezamzadeh-Ejhieh. *Desalination Water Treat*, **166**(2019):92–104, .
DOI: https://doi.org/10.5004/dwt.2019.24638.

[51] R. Sheikhsamany and A. Nezamzadeh-Ejhieh. *J. Mol. Liq.*, **414**(2024):126265.
DOI: https://doi.org/10.1016/j.molliq.2024.126265.

[52] R. Sheikhsamany, A. Nezamzadeh-Ejhieh, and R. S. Varma. *J. Surf. Interface*, **54**(2024):105205.
DOI: https://doi.org/10.1016/j.surfin.2024.105205.

[53] A. Pourtaheri and A. Nezamzadeh-Ejhieh. *Chem. Eng. Res. Des.*, **104**(2015):835–843.
DOI: https://doi.org/10.1016/j.cherd.2015.10.031.

[54] F. Soleimani and A. Nezamzadeh-Ejhieh. *J. Mater. Res. Technol*, **9(6)**(2020):16237–16251.
DOI: https://doi.org/10.1016/j.jmrt.2020.11.091.

[55] S. A. Mirsalari, A. Nezamzadeh-Ejhieh, and A. R. Massah. *Environ. Sci. Pollut. Res.*, **29(22)**(2022):33013–33032, .
DOI: https://doi.org/10.1007/s11356-021-17569-1.

[56] N. Mehrabanpour, A. Nezamzadeh-Ejhieh, S. Ghattavi, and A. Ershadi. *A., J. Appl. Surf. Sci.*, **614**(2023):156252, .
DOI: https://doi.org/10.1016/j.apsusc.2022.156252.

[57] S. A. Mirsalari, A. Nezamzadeh-Ejhieh, and A. R. Massah. *Spectrochim. Acta A Mol. Biomol. Spectrosc*, **288**(2023):122139, .
DOI: https://doi.org/10.1016/j.saa.2022.122139.

[58] S. D. Khairnar and V. S. Shrivastava. *J. Taibah Univ. Sci.*, **13(1)**(2019):1108–1118, .
DOI: https://doi.org/10.1080/16583655.2019.1686248.

[59] R. S. Shinde, V. A. Adole, S. D. Khairnar, P. B. Koli, and T. B. Pawar. *Inorg. Chem. Commun*, **170**(2024):113206.
DOI: https://doi.org/10.1016/j.inoche.2024.113206.

[60] S. D. Khairnar and V. S. Shrivastava. *SN Appl. Sci.*, **1(7)**(2019):762, .
DOI: https://doi.org/10.1007/s42452-019-0761-4.

[61] N. Mehrabanpour, A. Nezamzadeh-Ejhieh, and S. Ghattavi. *Environ. Sci. Pollut. Res.*, **30(2)**(2023):5089–5102, .
DOI: https://doi.org/10.1007/s11356-022-22557-0.

[62] N. Mehrabanpour, A. Nezamzadeh-Ejhieh, and S. Ghattavi. *Environ. Sci. Pollut. Res.*, **30(12)**(2023):33725–33736, .
DOI: https://doi.org/10.1007/s11356-022-24613-1.

[63] P. Hemmatpour and A. Nezamzadeh-Ejhieh. *Chemosphere*, **307**(2022):135925.
DOI: https://doi.org/10.1016/j.chemosphere.2022.135925.

[64] S. Salesi and A. Nezamzadeh-Ejhieh. *Environ. Sci. Pollut. Res.*, **29(60)**(2022):90191–90206.
DOI: https://doi.org/10.1007/s11356-022-22100-1.

[65] A. Nezamzadeh-Ejhieh and Z. Banan. *Iran. J. Catal.*, **2(2)**(2012): 79–83.

[66] S. D. Khairnar, A. N. Kulkarni, S. G. Shinde, S. D. Marathe, Y. V. Marathe, S. D. Dhole, and V. S. Shrivastava. *J. Photochem. Photobiol*, **6**(2021):100030, .
DOI: https://doi.org/10.1016/j.jpap.2021.100030.

[67] Y. H. Chiu, T. F. M. Chang, C. Y. Chen, M. Sone, and Y. J. Hsu. *Catalysts*, **9**(2019):430.
DOI: https://doi.org/10.3390/catal9050430.

[68] Y. V. Marathe, M. M. V. Ramanna, and V. S. Shrivastava. *Desalination Water Treat*, **51(28-30)**(2013):5813–5820.
DOI: https://doi.org/10.1080/19443994.2013.769720.